Classification: PHYSICAL SCIENCES, Applied Physical Sciences

Title: Synchronized structure and surface tension measurement on individual secondary aerosol particles by low-voltage transmission electron microscopy

Authors: Fangyuan Zheng[1,2+], Wai Chung Lam[1+], Ka Hei Lai[1+], Lok Wing Wong[1,2], Yisong Zhang[1], Zhangyuan Yan[1], Chak Chung Sham[1], Quoc Huy Thi[3,4], Thuc Hue Ly[3,4*], Jiong Zhao[1,2*]

Affiliations:

[1] Department of Applied Physics, The Hong Kong Polytechnic University, Kowloon, Hong Kong, China.

[2] The Hong Kong Polytechnic University Shenzhen Research Institute, Shenzhen, China.

[3] Department of Chemistry and Center of Super-Diamond & Advanced Films (COSDAF), City University of Hong Kong, Kowloon, Hong Kong, China.

[4] City University of Hong Kong Shenzhen Research Institute, Shenzhen, China.

[+] These authors contribute equally to this work.

*Correspondence to: thuchly@cityu.edu.hk, jiongzhao@polyu.edu.hk

Zheng, F., Lam, W. C., Lai, K. H., Huang, L., Wong, L. W., Zhang, Y., ... & Zhao, J. (2020). Synchronized Structure and Surface Tension Measurement on Individual Secondary Aerosol Particles by Low-Voltage Transmission Electron Microscopy. Environmental Science & Technology Letters, 7(8), 560-566.

Abstract:

A number of physical and chemical models have been built to describe the secondary aerosols (SAs) in atmosphere, however, the direct experimental approaches to simultaneously characterize the chemical structures and physical properties on the single-particle level is lacking. It obscures the understanding of SAs formation mechanisms, and impedes the development on the accurate prediction and control of air pollution. Here we obtained the clear core-shell structural information of the aqueous aerosols employing low-voltage transmission electron microscopy-energy dispersive spectroscopy (TEM-EDS). Meanwhile, the prevalent 10-20% surface tension reduction due to organic matter partitioning has been unveiled. Further analysis and modelling shows that smaller SAs can yield greater surface tension reduction, whilst the pronounced surface tension reduction may enlarge the size of SAs up to 50%. Our work paves the way to the unprecedented comprehensive single-particle study on the global atmospheric SA problems.

Key words: secondary aerosol particles, structure and surface tension, transmission electron microscopy.

Significance: Air pollution is raising more and more attention nowadays, in which the ultrafine atmospheric aerosols play an important role. Due to the size in nanoscale and multiplex chemical composition, the cognition of structure and formation mechanisms of secondary aerosols is still limited. Taking advantage of high magnification and elements analysis of transmission electron microscopy, we are able to obtain the clear core-shell structural information and study the structure as well as surface tension with modeling. The results not only establish a comprehensive way to analyze the individual secondary aerosol particles, but also provide a deeper understanding of global atmospheric problem processing.

Introduction:

The ultrafine atmospheric aerosols strongly contribute to the urban air pollution today. The atmospheric aerosols impact the human health (through inhalation or precipitation), the visibility outdoors, the global radiation balance and climate change (1), etc. Despite studied for decades, to date the matter partitioning in aerosols with their nucleation and growth mechanisms are still elusive (2). The aqueous secondary aerosols (SA) are particularly interesting for their worldwide presence and the complex physical and chemical processes involved (3). The non-volatile solutes in aqueous aerosols can lead to the surface activity suppression (known as Raoult's effect) (4), favoring the accelerated growth in size. In contrast, the impact of surface tension variation in aerosols was overlooked for a long time. Recently the surface tension reduction by organic matter partitioning has been addressed in high altitude SA for the cloud condensation (5). In comparison, aerosols in near-ground atmosphere are more under-saturation and deeply influenced by the biosphere and anthropogenic activities.

Herein, we suggest the non-negligible reduction in surface tension plays a key role in the formation and growth of near-ground aqueous SAs. Although it is challenging to measure the surface tension of the ultrafine SAs directly, in our field campaign, the surface tension reduction was derived from the organic matter partitioning measured on single-particle level by the transmission electron microscopy (TEM), scanning transmission electron microscopy (STEM) and chemical analysis.

The prevalent ten to twenty percent reduction in surface tension retrieved from our field dataset is in line with the classic Köhler theory (6). The pronounced surface tension reduction can enlarge the SA sizes up to 50% in a wide diameter range (0.2~1 μm). Meanwhile, a minimum surface tension reduction in SAs is rendered by the leverage of water and non-volatile solute uptake. Our work clearly manifests that surface tension variation originated from organic matter needs to be counted in the previous near-ground aerosol models (7-9) for more accurate prediction of the near-ground particulate matter (PM) concentration and the air pollution levels.

As revealed by the previous studies (10), the near-ground atmospheric SAs are usually comprised of both organic and inorganic matter (Fig. 1*A*). While the thermodynamics of inorganic aerosols can be satisfactorily explained by the classic Köhler theory (6), currently the organic aerosols have been illustrated by a variety of models for the organic matter partitioning and phase separation (11). In the lab or field studies on the SAs, the optical spectroscopy and mass spectrometry methods for atmospheric chemistry (12) have been well established. However, due to the lack of single-particle resolved data in previous studies, the structures, phase distributions and solute partitions of SAs are still under dispute. In particular, the surface tension, which results from the solute/phase partitioning and directly relevant to the thermodynamic energy, is virtually a key factor governing the micro-physics of SAs.

Nowadays the electron microscopies including transmission electron microscopy (TEM) and scanning TEM (STEM) (13) equipped with energy dispersive spectroscopy (EDS) have been widely exploited for high spatial resolution imaging and in-parallel chemical analysis. The recent advent of low-voltage and aberration-corrected TEM/STEM (14), as well as the multiple-detector EDS (15) has achieved atomic resolution on the beam-sensitive specimens. As being presented in the following, the structure and chemical compositions in the atmospheric SAs measured by analytical TEMs, at single-particle level, can facilitate the unprecedented, combined and quantitative chemical and physical analysis on the SAs.

Results:

The field campaign on the near-ground atmosphere was carried out in urban Hong Kong, from January until July 2019. The sampling methods and weather conditions are described in *SI Appendix*, Table S1. The collected SA particles were directly analyzed by TEM/STEM. Combining the TEM/STEM images and energy dispersive spectroscopy (EDS), three major classes of PM can be distinctly identified, named the carbon soot (graphitic onion-like carbon), inorganic particle (e.g. SiO_x and FeO_x) (*SI Appendix*, Fig. S1) and hygroscopic SAs. The representative TEM images for the morphology of hygroscopic SAs are shown in Fig. 1*B*, while lower magnification image is shown in *SI Appendix*, Fig. S2. In most of our samples, hygroscopic SAs contribute the dominant portion in near-ground PM according to the field study results (*SI Appendix*, Table S2), in consistent with the environment conditions in Hong Kong, i.e., high humidity, high temperature and high anthropogenic carbonaceous emission (16,17). Based on statistical results on the SAs, the particle counts/fractions are shown in Fig. 1*C*, therefore, higher humidity environment can significantly enlarge the size of SAs.

Under normal operation of TEM/STEMs, high spatial resolution imaging and chemical analysis are easy to damage the sensitive specimens such as the aerosols here, therefore, we applied the low voltage STEM-EDS to acquire the data which is for quantification in next stage. It is noteworthy that the low-voltage aberration-corrected STEM method is approaching atomic sensitivity during EDS analysis. Upon close inspection on the EDS mapping results of SAs here, the majority of SA particles exhibit clear core-shell separations in the dry remnant form (Fig. 2, *A* to *C*). The shells mainly consist of carbon (C), nitrogen (N), oxygen (O), and silicon (Si) appears in the outmost layers; whereas the inner cores contain N, O, sulfur (S), sodium (Na), potassium (K) and chlorine (Cl). These major elements are possibly contributed by the sea water cycle and the massive secondary photocatalytic reaction products—ammonia sulfate (18,19). Other minor elements such as aluminum (Al), calcium (Ca), iron (Fe), magnesium (Mg) and zinc (Zn) are occasionally found in the cores (more examples shown in *SI Appendix*, Fig. S3). Quantitative EDS mapping on the partitioning in single particles are presented in Fig. 2, *D* and *E*, and *SI Appendix*, Fig. S4. Under the sampling condition for SAs shown in Fig. 2, the weight ratio of the C/O/N in the shell is ca. 10/2/1, implying a high oxidation and hygroscopic nature in SAs (20,21).

As the distinct organic-inorganic core-shell separation measured above, the surface dominant partition of non-volatile organic matter in SAs in our field campaign is confirmed. Oxidation, nitration, and sulfurization serve as potential reaction paths (19). The extensive sun-light exposure, catalytic effects of the surface organic shell and the oxidative solutes dissolved in the aqueous SAs accelerates the underlying conversion. The original hydrophobicity in the carbonaceous matter (low O, N and S content) thereby turns into the hydrophilic (high O, N and S content), leading to the significantly enhanced water intake in SAs.

It is worth noting the SAs we observed in TEM are water-exclusive (dried), as the SAs collide and be captured on the carbon films (sample collector), two water evaporation modes are allowed, (i) the peripheral shrinking (PS) mode and (ii) the dome lowering (DL) mode (Fig. 2*F*). In the PS mode the boundary of the SA particles shrinks inward with the decreasing volume via evaporation, while in the DL mode the boundary is fixed with the decreasing height of SA particles. The evaporation mode is associated with the contact angle (θ) which is virtually determined by the surface tension (σ) of the SAs. In the initial stage of evaporation, σ increases by the continuous precipitation of the OM surfactant, as well as θ, until a maximum limit of σ_c is reached. As the evaporation kinetics is controlled by the thermodynamic equilibrium in the aqueous SAs, the stabilization of σ leads to suppression in evaporation speed, promoting the continuous precipitation of OM surfactant in the position-fixed boundary and forms a remnant OM ring (with diameter d_c) (Fig. 2*F*). In connection to the secondary OM ring, the DL mode starts. By continuous precipitation on the fixed SA boundaries in DL modes, the boundary between the PS and DL modes can be clearly identified (Fig. 2, *A* and *B*).

According to the TEM-EDS results, the precipitation order of the solutes in the SAs is from organics to inorganics. The most hydrophobic -SiH_3 and -SiO groups are leading, followed by the other OM predominantly partitioned to the outer boundaries of SAs. While the OM is absent in the core parts, which is unlikely if the OM presents in the bulk of SAs. In contrast, the inorganic ion solutes (Na^+, K^+, NH_4^+, SO_4^{2-}) precipitate homogeneously in the core part except some cases preferably attach to the heterogeneous nuclei particles. These bulk inorganic solutes are not involved in the initial PS mode evaporation but precipitate after the critical surface tension (σ_c) is reached in the second DL mode evaporation stage.

The surface tension for individual particles in each stage is monotonically dependent on the amount of OM surfactant precipitation below the critical micelle concentration (CMC) (22),

$$\sigma = \sigma_0 - \mathrm{k}\ln(c), \tag{1}$$

where c is the OM concentration, k is constant, σ_0 is the surface tension of water. Thereby the surface tension and reduction in it is measurable by our TEM-EDS experiment through quantitative integration of EDS intensity of carbon in the shell layer (see Methods). It should be noted that the lowering in σ is normalized by the maximum σ reduction in our analysis for more than a hundred SA particles measured by TEM. If we apply the original contact angle between water and the amorphous carbon film (ca. 40°), the maximum reduction of surface tension in our measured SA particles can reach 24% (completely wetting between SA particles and amorphous carbon TEM grid), corresponding to the highest reduction (-1.0) in surface tension for SA diameters around 200 nm (Fig. 3*A*). Usually a surface tension reduction between 10% ~ 20% is rendered by our measurement for SAs between 0.2~1.6 μm, and a clear size dependence (bigger SAs yield less surface tension reduction) is observed.

The distinct size dependence of the surface tension reduction in SAs can be understood by the hygroscopic growth of the SAs which dilutes the surfactant content to increase the surface tension. However, the surface tension has a clear saturation tendency at around -0.4, corresponding to SA diameters larger than 1 μm (Fig. 3*A*). It is in agreement with the saturation for TEM grid-captured

SA samples at the transition from “PS” to “DL” modes (the OM at the fixed boundaries is counted here) for SAs with all critical diameters (d_c) (Fig. 3*B*). It is caused by the thermodynamic equilibrium between the water and inorganic solute intake. Furthermore, the statistical analysis results from the surface tension reduction under different super-saturation (humidity) and different OM content/nuclei in the atmosphere (morning, noon and evening) are shown in Fig. 3, *C* and *D*. The low humid environment and evening samples have more significant surface tension reduction.

The surface tension reduction indeed has direct impact on the SA size distribution. With the amount of the non-volatile inorganic solutes (including Na, K, N, S, Cl) measuring from the TEM-EDS results, the experimentally obtained hygroscopic radius-bulk (inorganic) solute partition relationship can be fitted with the classic Köhler model (see methods) (6), excluding (Fig. 4*A*) or including (Fig. 4*B*) the measured surface tension reduction. It is evident that large deviations from the classic model exist in the experimental results without the surface tension reduction for different size SA particles, while the model including the measured surface tension reduction can fit much better with the measured size dependences for the inorganic solute mass of SAs. The rise of SA sizes originated from the surface tension reduction reaches up to ca. 50%. Accordingly, the results under different humidity in the field campaign, i.e., the humidity (super-saturation) dependence of the hygroscopic radius are presented in Fig. 4*C*. The significant effect of the surface tension depression by the OM precipitation is clearly manifested for all the weather conditions.

Furthermore, the result shows the mean size of the SAs has correlation with the mean O/C atomic ratio in the shell layer of hygroscopic SAs (acquired under different weather conditions, see *SI*

Appendix, Fig. S5). Greater randomness/S.D. lies in the high OM concentration (high O/C ratio) side (yield smaller SAs accordingly), probably caused by the enhanced (saturated) viscosity or even the “glassy state” (23,24) on the surface shells under the condition of ultra-high OM surface partition for the ultra-small particles. This might be influenced by the temperature and sun-light exposure environment as well, which can trigger the oligomerization and mechanical hardening in the shell of SAs. In addition, it is also found the S content is often higher in the shell layer for the smaller and glassy particles (*SI Appendix*, Fig. S6), while the formation mechanism behind this is currently under investigation.

Conclusion:

To conclude, our field campaign and specific TEM-EDS analysis on the single-particle level directly visualized and confirmed the surface favorable partitioning of OM in the near-ground SAs. More importantly, through the quantitative chemical analysis along with the measurement of surface tension according to the OM and inorganic solute contents, the surface tension reduction/suppression effect has been completely understood in the context of classic Köhler model, also incorporated into the hygroscopic thermodynamics of the air/SA system. Therefore, our analytical high resolution TEM approach for SA field studies has opened an avenue for unprecedented comprehensive understanding of the chemical and physical properties of the atmospheric SAs.

Materials and Methods:

Sample collections

The samples of near-ground particulate matters (PM) were collected in Hung Hom, Hong Kong, from January to July 2019. Each set of samples contained three PM samples, which were taken in three different time slots in a day. For consistency, these PM samples were taken at the same location in the same time slots. The sampling site was the footbridge extended from the main campus of the Hong Kong Polytechnic University in Hung Hom. The other side of the site is the Cross Harbour Tunnel across the Victoria Harbour. Therefore, PMs were able to flow from the sea to the sampling site through a sea breeze. Another characteristic is that the road near this site is heavily trafficked every day, leading to high population of PMs on the near-ground level. To evaluate the changes of PMs in various weather conditions, three PM samples were collected in a day with three time slots: morning (10:00), afternoon (14:00) and evening (18:00). Meteorological factors, including ambient temperature (AT), relative humidity (RH) and visibility, were recorded.

Sampling method

A near-ground PM sample was collected by a quantifoil^{TM} TEM grid, with the type of the grid R 1.2/1.3. Besides the grid, a PM particle counter (DT-9880, CEM) was used for collecting and counting PM levels on the TEM grid. After the TEM grid is mounted at the particle entrance, the particle counter was turned to the side of Cross Harbour Tunnel and started to collect PMs. It took fifteen minutes for collecting each PM sample, to ensure PMs are effectively captured on the grid.

TEM analysis

The near-ground PMs were analyzed by the transmission electron microscopy (TEM)/ scanning transmission electron microscopy (STEM) using JEOL 2100F (accelerating voltage at 200 kV) and JEM-ARM200F (accelerating voltage at 60 kV) equipped with double EDX detectors. TEM images under the magnification of 10000X (low mag) demonstrated the overview of samples. High-resolution of the PM (high magnification) images were allowed to investigate the morphology and chemical composition of a single particle in a PM sample. In specific, the JEM-ARM200F transmission electron microscope (TEM) retrofitted with a CEOS spherical (Cs) aberration corrector was used. The accelerating voltage (60 kV) and exposure time has been minimized to reduce the electron beam damage on the sample. The vacuum value during measurement was better than 1.5×10^{-7} mbar, together with the electron beam current of ca. 13 μA. At the time of performance, the scanning probe size was 1.5 Å. The acquisition time of STEM-HAADF image was 19 μs per pixel in order to minimize electron beam damage. The 512 × 512 pixel images were acquired with the CL aperture of 40 μm and the range of collection angle was 45 to 180 mrad.

EDS mapping and element quantification

EDS mapping was performed by the dry-SDD Dual EDS system run by automatic software (Analysis Station) provided by JEOL. The serial element distribution data for each shell layer (by subtraction of two circled area) are extracted on single SA particle level. The total atomic weight/mass of C and O element mapping are counted for OM partition and subsequent surface tension lowering according to eq.1, while total atomic weight/mass of Na, K, S, N, Cl are counted for inorganic matter partition and subsequent thermodynamic analysis, according to Kohler theory[6]: $\mathrm{S} = 1 + \frac{\mathrm{a}\sigma}{r} - \frac{\mathrm{b}m}{r^2}$, where S is the saturation (fixed in one sample), a, b are two constants, m is the inorganic solute mass, and r is the radius of particle.

Data Availability: All data are available within the main text and *SI Appendix*.

Acknowledgements:

This work was supported by the Hong Kong Research Grant Council under Early Career Scheme (Project No.25301018, 21303218), City University of Hong Kong (Project No. 9610387), National Science Foundation of China (Project No. E010701), and Shenzhen Science and Technology Innovation Commission (Project No. JCYJ20170818104717087). Z.F., L.W.C. and L.K.H. contributed equally in this work. Z.J. and L.T.H. conceived and led the project. Z.F., L.W.C. L.K.H. collected samples, conducted the sample characterizations and TEM experiments. W.L.W., Z.Y, Y.Z, C.S.C., T.Q.H. assisted in data analysis. All the authors discussed the MS and agreed on its contents.

References:

1. B. Ervens, B. J. Turpin, R. J. Weber, Secondary organic aerosol formation in cloud droplets and aqueous particles (aqSOA): a review of laboratory, field and model studies. *Atmospheric Chemistry and Physics*, **11**, 11069-11102 (2011).

2. J. Tröstl *et al.,* The role of low-volatility organic compounds in initial particle growth in the atmosphere. *Nature*, **533**, 527 (2016).

3. M. Shiraiwa *et al.,* Global distribution of particle phase state in atmospheric secondary organic aerosols. *Nature communications*, **8**, 15002 (2017).

4. R. Sorjamaa *et al.,* The role of surfactants in Köhler theory reconsidered. *Atmospheric Chemistry and Physics*, **4**, 2107-2117 (2004).

5. J. Ovadnevaite *et al.,* Surface tension prevails over solute effect in organic-influenced cloud droplet activation. *Nature*, **546**, 637 (2017).

6. H. Köhler, The nucleus in and the growth of hygroscopic droplets. *Transactions of the Faraday Society*, **32**, 1152-1161(1936).

7. T. D. Vaden, D. Imre, J. Beránek, M. Shrivastava, A. Zelenyuk, Evaporation kinetics and phase of laboratory and ambient secondary organic aerosol. *Proceedings of the National Academy of Sciences*, **108**, 2190-2195 (2011).

8. A. Tandon, N. E. Rothfuss, M. D. Petters, The effect of hydrophobic glassy organic material on the cloud condensation nuclei activity of particles with different morphologies. *Atmospheric Chemistry and Physics*, **19**, 3325-3339 (2019).

9. S. Li, S. Cheng, L. Du, W. Wang, Establishing a model organic film of low volatile compound mixture on aqueous aerosol surface. *Atmospheric environment*, **200**, 15-23 (2019).

10. Y. S. Djikaev, E. Ruckenstein, Formation and evolution of aqueous organic aerosols via concurrent condensation and chemical aging. *Advances in colloid and interface science,* **265**, 45-67 (2019).

11. D. K. Farmer, C. D. Cappa, S. M. Kreidenweis, Atmospheric processes and their controlling influence on cloud condensation nuclei activity. *Chemical Reviews*, **115**, 4199-4217 (2015).

12. P. F. DeCarlo *et al.,* Field-deployable, high-resolution, time-of-flight aerosol mass spectrometer. *Analytical chemistry*, **78**, 8281-8289 (2006).

13. K. F. Ho *et al.,* Characterization of chemical species in PM2. 5 and PM10 aerosols in Hong Kong. *Atmospheric Environment*, **37**, 31-39 (2003).

14. T. Sasaki *et al.,*Performance of low-voltage STEM/TEM with delta corrector and cold field emission gun. *Journal of Electron Microscopy*, **59(S1)**, S7-S13 (2010).

15. W. Xu, J. H. Dycus, X. Sang, J. M. LeBeau, A numerical model for multiple detector energy dispersive X-ray spectroscopy in the transmission electron microscope. *Ultramicroscopy*, **164**, 51-61 (2016).

16. Y. Cheng *et al.,* PM2. 5 and PM10-2.5 chemical composition and source apportionment near a Hong Kong roadway. *Particuology*, **18**, 96-104 (2015).

17. Q. Yang, Q. Yuan, T. Li, H. Shen, L. Zhang, The relationships between PM2. 5 and meteorological factors in China: Seasonal and regional variations. *International journal of environmental research and public health*, **14**, 1510 (2017).

18. C. R. Ruehl, K. R. Wilson, Surface organic monolayers control the hygroscopic growth of submicrometer particles at high relative humidity. *The Journal of Physical Chemistry A*, **118**, 3952-3966 (2014).

19. M. Hallquist *et al.,* The formation, properties and impact of secondary organic aerosol: current and emerging issues. *Atmospheric chemistry and physics*, **9**, 5155-5236 (2009).

20. M. Kuwata, S. R. Zorn, S. T. Martin, Using elemental ratios to predict the density of organic material composed of carbon, hydrogen, and oxygen. *Environmental science & technology*, **46**, 787-794 (2011).

21. A. K. Bertram *et al.,* Predicting the relative humidities of liquid-liquid phase separation, efflorescence, and deliquescence of mixed particles of ammonium sulfate, organic material, and water using the organic-to-sulfate mass ratio of the particle and the oxygen-to-carbon elemental ratio of the organic component. *Atmospheric Chemistry and Physics*, **11**, 10995-11006 (2011).

22. A. F. Belhaj *et al.,* Experimental Investigation of Surfactant Partitioning in Pre-CMC and Post-CMC Regimes for Enhanced Oil Recovery Application. *Energies*, **12**, 2319 (2019).

23. A. Virtanen *et al.,* An amorphous solid state of biogenic secondary organic aerosol particles. *Nature*, **467**, 824-827. (2010).

24. T. Koop, J. Bookhold, M. Shiraiwa, U. Pöschl, Glass transition and phase state of organic compounds: dependency on molecular properties and implications for secondary organic aerosols in the atmosphere. *Physical Chemistry Chemical Physics*, **13**, 19238-19255 (2011).

Figures and Figure captions

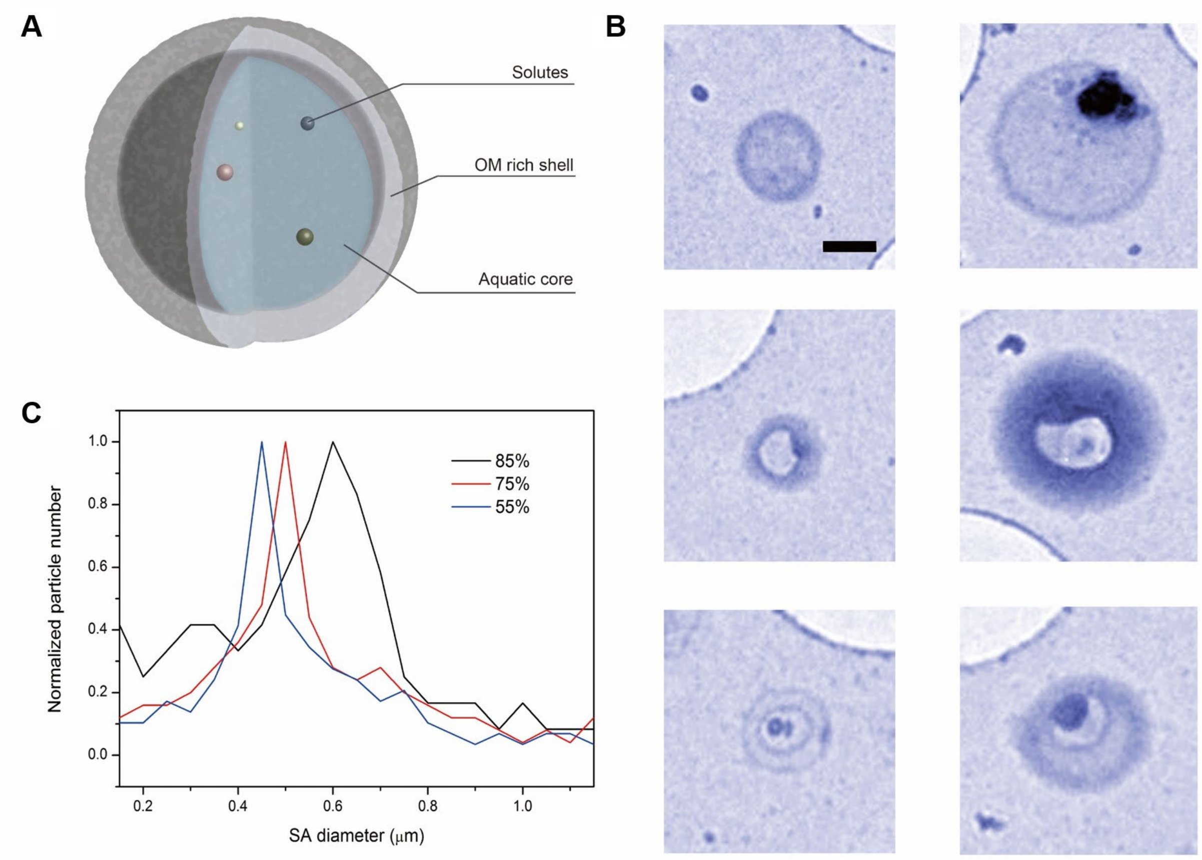

Fig. 1. The aqueous SA particles collected in field campaign. (*A*) The scheme of the SAs. (*B*) TEM images for typical SAs, scale bar =100 nm for all the images. (*C*) The size distributions of the SAs under different super-saturations (marked on upper-right side).

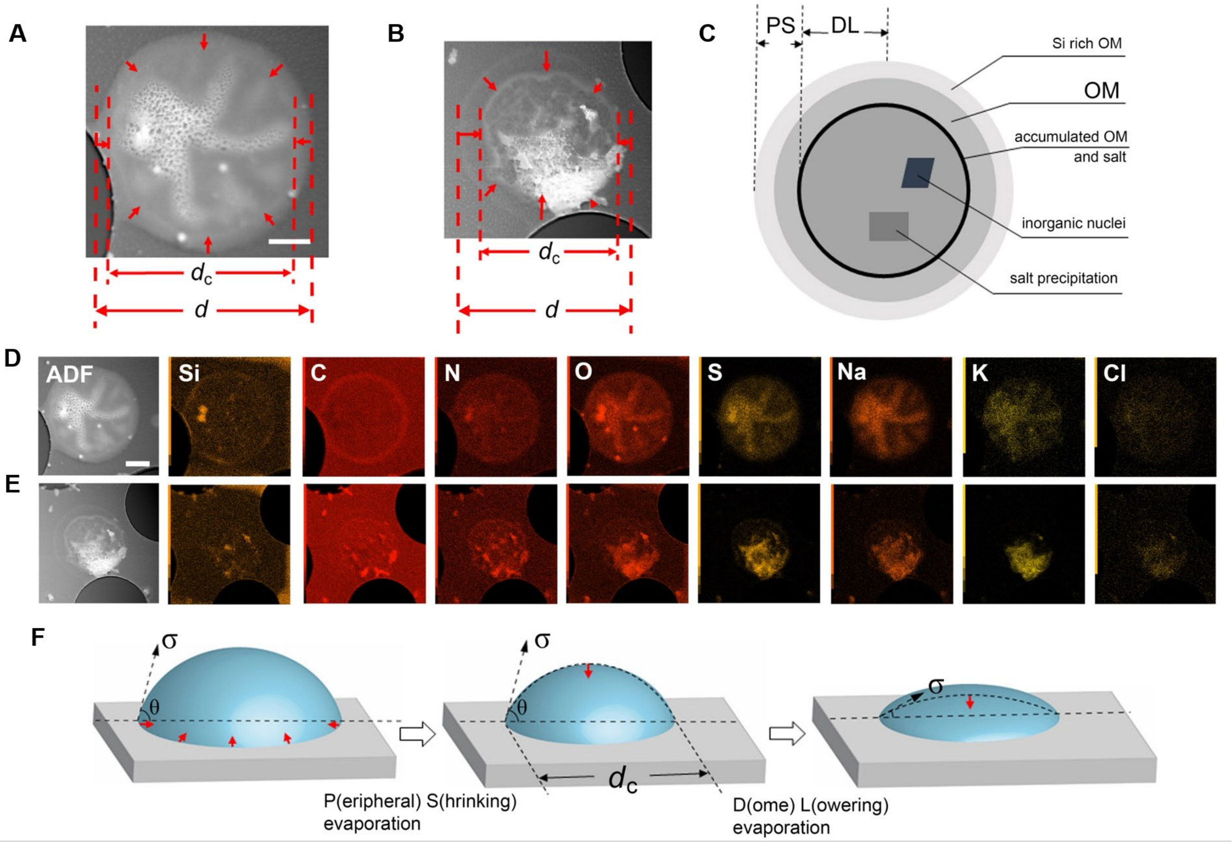

Fig. 2. The chemical and surface tension analysis on SAs via LV-TEM. (*A*), (*B*) The high angle annular dark field (HAADF) images for typical SAs. *d* and d_c indicate the original and critical (PS-DL transition) boundaries. Scale bar =200 nm in (*A*), also apply for (*B*). (*C*), Scheme of the precipitation order of the different solutes. (*D*), (*E*) The EDS analysis results for typical SAs in (*A*), (*B*). Scale bar =200 nm for (*D*), (*E*). (*F*) The Schematic evaporation process of the SAs (from PS to DL mode).

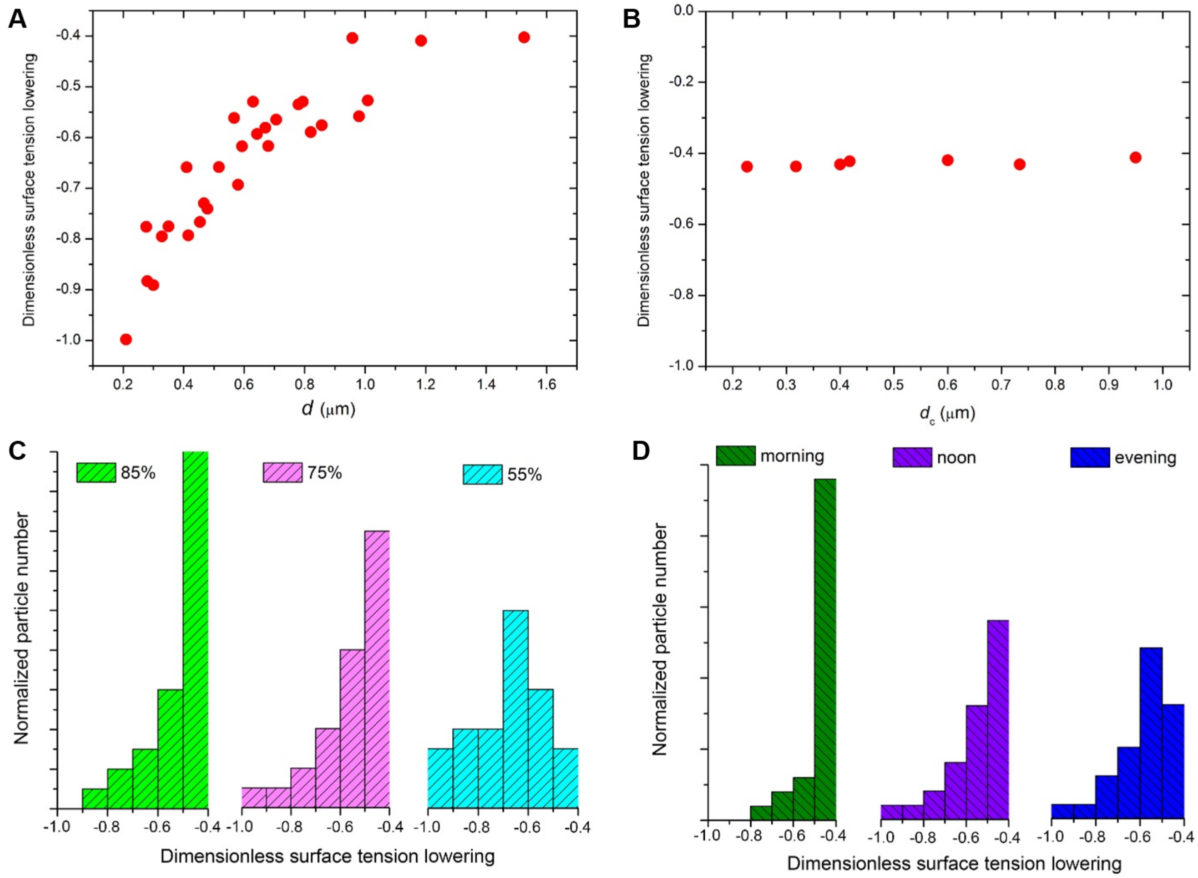

Fig. 3. The measured surface tension reduction. (*A*) The surface tension reduction versus SA diameter plot (sampling time: 08/01/2019, see *SI Appendix*, Table S1). (*B*) The instant surface tension reduction measured at the critical diameter (PS to DL mode transition) in different particles with same condition as in (*A*). (*C*) The surface tension lowering measured under different super-saturation (85%, 75% and 55%). (*D*) The surface tension lowering measured under different OM content in atmosphere (sampling at different time in 08/01/2019, see *SI Appendix*, Table S1).

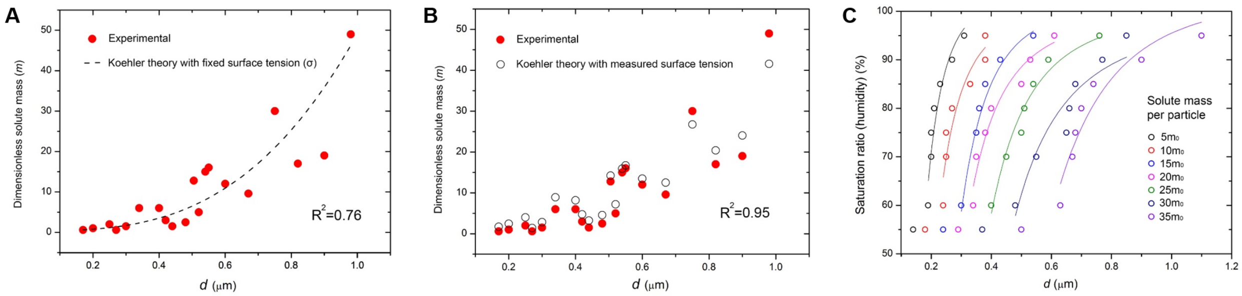

Fig. 4. Thermodynamics of SAs. (*A*) The total solute mass versus diameter plot, with Kohler theory model fitting (dashed line), using a fixed surface tension. (*B*) The same plot as (*A*), using our measured surface tension for each particle during fitting (open black circles). (*C*) The humidity versus SA diameter plot with different solute mass loading, fitted by the Kohler curves.